Annual Progress Report
February 12, 1999 - February 11, 2000

ABSTRACT

The purpose of this investigation is to develop a new model for the acceleration of the fast solar wind by nonlinear, time-dependent multidimensional MHD simulations of waves in solar coronal holes. Computational studies indicate that nonlinear waves are generated in coronal holes by torsional Alfvén waves. These waves in addition to thermal conduction may contribute considerably to the accelerate the solar wind. Specific goals of this proposal are to investigate the generation of nonlinear solitary-like waves and their effect on solar wind acceleration by numerical 2.5D MHD simulation of coronal holes with a broad range of plasma and wave parameters; to study the effect of random disturbances at the base of a solar coronal hole on the fast solar wind acceleration with a more advanced 2.5D MHD model and to compare the results with the available observations; to extend the study to a full 3D MHD simulation of fast solar wind acceleration with a more realistic model of a coronal hole and solar boundary conditions. The ultimate goal of the three year study is to model the fast solar wind in a coronal hole, based on realistic boundary conditions in a coronal hole near the Sun, and the coronal hole structure (i.e., density, temperature, and magnetic field geometry) that will become available from the recently launched SOHO spacecraft. We report on our study of the effects of slow magnetosonic waves recently detected by EIT on the solar wind.

1. Introduction

To account for the observed properties of the solar wind Alfvén waves were suggested as a source of momentum and heat, and studied in the linear regime (e.g., Alazraki & Courtier 1971, Belcher 1971, Hollweg 1973, Jacques 1977, Davila 1985, Davila 1987, Ofman & Davila 1995). The WKB approximation is the standard approach to study the effect of the Alfvén waves on the solar wind. Recent linear models include many realistic features and consider the propagation of three-dimensional Alfvén in a stratified, thermally conductive solar wind with WKB and non WKB fluctuations.

In order to consider fully the solar wind acceleration by transverse Alfvén waves, nonlinear effects must be included. This is necessary in order to couple the transverse

motions and the gradients of the magnetic pressure into the longitudinal motions. Nonlinear two-fluid one-dimensional MHD solar wind model with WKB Alfvén waves were developed and compared favorably with observations (e.g., Esser et al. 1997). However, with the WKB approach the Alfvén waves are not treated self consistently with the solar wind. Nonlinear effects due to the Alfvén waves in the solar wind, such as fast and slow waves were deduced from the second order analysis of the MHD equations (Lou 1993). Recently, self consistent nonlinear computations of the solar wind acceleration by Alfvén waves were performed in one spatial dimension (Lau and Siregar 1996, Boynton & Torkelsson 1996) and in two dimensions (Ong et al. 1997, Ofman & Davila 1997a, Ofman & Davila 1998).

Ofman and Davila (1997a, 1998) (hereafter, OD) investigated the self-consistent nonlinear effects due to Alfvén waves in coronal holes via numerical solution of the nonlinear 2.5-D (3-D with azimuthal symmetry) resistive MHD equations in a spherical geometry with an (r, θ)-inhomogeneous atmosphere and the hydrostatic initial state. They found that solitary waves are driven by the Alfvén waves in a stratified coronal hole. Ofman and Davila (1997b) suggested that the solitary waves may explain the apparent broadening of ion emission lines observed by the SOHO Ultraviolet Coronagraph Spectrometer (UVCS). The waves that OD found propagate in a highly inhomogeneous radially divergent, dispersive, and dissipative medium, and are more complex than the classical sound solitons. Therefore, we refer to them as large amplitude nonlinear (LAN) waves.

Ofman, Nakariakov, & DeForest (1999) studied the propagation of slow magnetosonic waves in plumes using the inviscid 1D linear wave equation, and the nonlinear 2D MHD code in spherical geometry and found good qualitative agreement with the observed spatial and temporal evolution of the fluctuations in plume brightness obtained by EIT.

The compressive viscosity coefficient, as calculated using Braginskii's theory (Braginskii 1965) in the solar corona is many orders of magnitude larger than the shear viscosity coefficient (Porter, Klimchuk, & Sturock 1994, Ofman, Davila, & Steinolfson 1994) and should strongly damp the propagation of the slow magnetosonic waves. For typical coronal parameter, we find that the slow waves with frequencies in the few millihertz range will be dissipated within one solar radius above the photosphere.

The contribution of the low frequency slow waves to heating depends on the amount of energy flux available in these waves. The prevailing view based on Doppler shift observations (Athay & White 1979) is that a slow wave energy flux of $\sim 10^4$ erg cm^{-2} s^{-1} that reaches the corona is not sufficient to balance the coronal energy losses. However, Porter, Klimchuk, & Sturock claim that if the observed nonthermal Doppler broadening of 20-60 km s^{-1} of coronal emission lines (see, for example recent measurements of nonthermal line widths with the SUMER instrument on SOHO reported by Warren et al. 1997, and

Chae, Schuhle, & Lemaire 1998) is attributed to slow waves, than the energy flux is greatly underestimated. The direct observation of slow magnetosonic waves in plumes by EIT (e.g., DeForest and Gurman 1998) lends some support to the latter view.

2. Results

2.1. Dissipative Slow Magnetosonic Waves in Plumes

2.1.1. Dissipative MHD Model Equations

The main goal of the present numerical simulation of the slow magnetosonic waves in plumes is to investigate the role of dissipation, plume structure, and nonlinearity on the propagation of the waves. For this purpose we model the polar plume in the $r-\theta$ plane with a 2D MHD nonlinear code in spherical geometry, where r is along the solar radial direction ($r=1$ is the coronal boundary), and θ is the latitudinal direction. We include viscous (compressive) and resistive dissipation, and the polytropic energy equation. We set the polytropic index γ equal to 1. We plan to use more realistic energy equation in our future studies.

The normalized MHD equations are

$$\frac{\partial \rho}{\partial t} + \nabla \cdot (\rho \mathbf{v}) = 0, \tag{1}$$

$$\frac{\partial \mathbf{v}}{\partial t} + (\mathbf{v} \cdot \nabla)\mathbf{v} = -\frac{E_u}{\rho}\nabla p - \frac{1}{F_r r^2} + \frac{\mathbf{J} \times \mathbf{B}}{\rho} - \frac{\nabla \cdot \Pi}{\rho}, \tag{2}$$

$$\frac{\partial \mathbf{B}}{\partial t} = \nabla \times (\mathbf{v} \times \mathbf{B}) + S^{-1}\nabla^2 \mathbf{B}, \tag{3}$$

$$\frac{\partial T}{\partial t} + \mathbf{v} \cdot \nabla T = (\gamma - 1)(S_v + S_r - T\nabla \cdot \mathbf{v}), \tag{4}$$

where Π is the viscous stress tensor (Braginskii 1965), S_v is the viscous heating term and S_r is the resistive heating term. When $\gamma = 1$ the source terms do not affect the temperature.

The quantities in the MHD equations are normalized with $r \rightarrow r/R_\odot$, $t \rightarrow t/\tau_A$, $v \rightarrow v/v_A$, $B \rightarrow B/B_0$, $\rho \rightarrow \rho/\rho_{00}$, $p \rightarrow p/p_0$. The physical parameters are the Lundquist number $S = \tau_r/\tau_A$, the resistive time scale $\tau_r = 4\pi R_\odot^2/\nu c^2$ (where ν is the resistivity, and c is the speed of light), the Alfvén time scale $\tau_A = R_\odot/v_A$, the Froude number $F_r = v_A^2 R_\odot/(GM_\odot)$ (where G is the gravitational constant, and $M_\odot$ is the solar mass), the Euler number $E_u = p_0/(\rho_{00}v_A^2) = C_s^2/v_A^2$ ($\equiv \beta/2$), the sound speed $C_s = \sqrt{\gamma p_0/\rho_{00}}$, the Alfvén speed $v_A = B_0/\sqrt{4\pi\rho_{00}}$. The values of the magnetic field B_0, pressure p_0, and density ρ_{00} are taken at the solar boundary of the plumes.

Here, we are interested in the dissipation of longitudinal waves. Therefor, we consider the radial component of the viscosity

$$(\nabla \cdot \Pi)_r = -\frac{4}{3}\eta_0 \left[\frac{\partial^2 v_r}{\partial r^2} + \left(\frac{\partial v_r}{\partial r} - \frac{v_r}{r} \right) \left(\frac{2}{r} + \frac{\partial \ln \eta_0}{\partial r} \right) \right] \tag{5}$$

where the compressive viscosity coefficient is given by (Braginskii 1965)

$$\eta_0 = 0.96 n k T_p \tau_p, \tag{6}$$

with the proton collision time given by

$$\tau_p = \frac{3\sqrt{m_p}(kT_p)^{3/2}}{4\sqrt{\pi} n \lambda e^4}. \tag{7}$$

In the above, m_p is the proton mass, T_p is the proton temperature, e is the electron charge, and $\lambda \approx 20$ is the Coulomb logarithm. For typical conditions at the base of the corona with $T_p = 1.4 \times 10^6$ K and $n = 5 \times 10^8$ cm^{-3} we get $\tau_p = 2.8$ s. The collision time is two orders of magnitude shorter than the typical slow wave period observed by EIT. At $1.2R_\odot$ the density drops by a factor of ~ 4 (assuming isothermal static atmosphere). This will result in ion collision time of 11 s, about 55 times smaller than the wave period observed by EIT. Thus, the plasma is in the collisional regime in the region of interest, and Landau damping can be neglected there. The proton collision frequency becomes comparable to the wave period (600 s) at about $3R_\odot$.

Note that the compressive viscosity coefficient varies mainly with temperature and can be written as $\eta_0 = \eta_{00} T_p^{5/2}$. In the present single-fluid MHD model we assume that that $T = T_p = T_e$, where T_e is the electron temperature, and we use the normalization $\eta_0 \rightarrow \eta_0/(R_\odot v_A \rho_{00})$. With this normalization we have $\eta_0 = \bar{\eta} C_s / v_A$.

The heating due to the compressive viscosity is given by

$$S_v = \frac{4}{3\rho}\eta_0 \left(\frac{\partial v_r}{\partial r} - \frac{v_r}{r} \right)^2. \tag{8}$$

We calculate and plot the radial heating rate $2\pi r^2 S_v$ for various cases discussed below.

2.1.2. Linear Theory of Slow Magnetosonic Waves in Viscous Fluid

Consider the linear 1D dynamics of slow magnetosonic waves propagating along the vertical magnetic field in an isothermal atmosphere. The magnetic field is taken to be

radially divergent. The atmosphere is spherically stratified by gravity with the equilibrium background density given by

$$\rho_0 = \rho_{00} e^{\left[-\frac{R_\odot}{H}(1-\frac{R_\odot}{r})\right]}, \tag{9}$$

where $R_\odot$ is the solar radius, and H is the scale height, defined as $H = 2k_B T R_\odot^2/(GM_\odot m_{\rm H})$ where k_B is Boltzmann's constant, T the temperature, G the gravitational constant, $M_\odot$ the Sun's mass and the hydrogen mass $m_{\rm H}$. The scale height can be estimated as $H(10^8{\rm cm}) \approx 61T(10^6{\rm K})$ (the factor in front of T is 51 when Helium is taken into account).

In spherical coordinates, the linear, spherical slow magnetosonic waves radially propagating strictly along the magnetic field, with perturbations of plasma density ρ and radial speed v_r, are governed by the equations

$$\frac{\partial \rho}{\partial t} + \frac{1}{r^2}\frac{\partial}{\partial r}\left(r^2 \rho_0 v_r\right) = 0, \tag{10}$$

$$\rho_0 \frac{\partial v_r}{\partial t} + C_s^2 \frac{\partial \rho}{\partial r} + g\rho - \frac{4}{3}\eta_0 \frac{\partial}{\partial r}\left[\frac{1}{r^2}\frac{\partial}{\partial r}(r^2 v_r)\right] = 0, \tag{11}$$

where $g = GM_\odot/r^2$ is the gravity acceleration and η_0 is the compressive viscosity coefficient, and C_s is the constant sound speed (see, § 2.1.1 below). Perturbations of the magnetic field and transversal components of the plasma velocity are not excited by the linear radially propagating slow wave considered.

Equations (10) and (11) can be combined into the wave equation

$$\rho_0 \frac{\partial^2 v_r}{\partial t^2} - C_s^2 \frac{\partial}{\partial r}\left[\frac{1}{r^2}\frac{\partial}{\partial r}(r^2 \rho_0 v_r)\right] - \frac{g}{r^2}\frac{\partial}{\partial r}(r^2 \rho_0 v_r) - \frac{4}{3}\eta_0 \frac{\partial}{\partial r}\left[\frac{1}{r^2}\frac{\partial}{\partial r}\left(r^2 \frac{\partial v_r}{\partial t}\right)\right] = 0. \tag{12}$$

Assuming solutions of the form $f(r)e^{-i\omega t}$ and writing the equation in terms of the density perturbation ρ gives

$$-\omega^2 \rho - \frac{C_s^2}{r^2}\frac{\partial}{\partial r}\left(r^2 \frac{\partial \rho}{\partial r}\right) - g\frac{\partial \rho}{\partial r} + i\frac{4}{3}\eta_0 \frac{C_s^2}{\omega \rho_0}\frac{\partial^4 \rho}{\partial r^4} = 0. \tag{13}$$

Since the viscosity is small we have used the ideal momentum equation to substitute for $\frac{\partial v_r}{\partial t}$ in the viscous term. The viscosity is only important in regions of high gradients. Therefore, we have kept only the highest order derivative of ρ in the viscous term. The solution of the wave equation is of the form

$$\rho \sim \frac{R_\odot}{r} e^{\left[-\frac{R_\odot}{2H}(1-\frac{R_\odot}{r})\right]} e^{ikz - i\omega t}, \tag{14}$$

where k is complex, and $z = r - R_\odot$. Expression (14) shows that the absolute amplitude of the density perturbations decreases with height, while the ratio of the density perturbations

amplitude (14) and the local equilibrium density value may grow provided that the viscosity is small ($Im(k_z) < R_\odot/2H$ near $r = 1R_\odot$),

$$\frac{\rho}{\rho_0} \sim \frac{R_\odot}{r} e^{\left[\frac{R_\odot}{2H}(1-\frac{R_\odot}{r})\right]} e^{ik\,z - i\omega\,t}. \tag{15}$$

In the isothermal inviscid atmosphere, the growth rate of the ratio ρ/ρ_0 depends on the temperature T only. In the presence of viscosity, the damping rate is subtracted from the growth rate (see the discussion at the end of § 2.1.3).

The approximate local dispersion relation of the dissipative waves is obtained by substituting the above solution (14) into the wave equation (13) and keeping only the largest terms

$$k \approx \frac{\omega}{C_s} - \frac{C_s^2 R_\odot^4}{8H^2 r^4} + i\frac{2}{3}\frac{\eta_0}{\rho_0}\frac{\omega^2}{C_s^3}. \tag{16}$$

The real part of this dispersion relation agrees with the ideal dispersion relation for spherical sound waves (Torkelsson, & Boynton 1998).

2.1.3. Nonlinear Slow Magnetosonic Waves

To understand basic physical mechanism responsible for the evolution of slow magnetosonic waves in the static, isothermal, spherically stratified atmosphere, we investigate weakly nonlinear dynamics of the waves under the assumption

$$\rho/\rho_0 \ll 1. \tag{17}$$

We restrict our attention to quadratically nonlinear processes only. Adding quadratically nonlinear terms to the right hand sides of Eqs. (10) and (11), we rewrite the equations as

$$\frac{\partial \rho}{\partial t} + \frac{1}{r^2}\frac{\partial}{\partial r}\left(r^2 \rho_0 v_r\right) = N_1, \tag{18}$$

$$\rho_0 \frac{\partial v_r}{\partial t} + C_s^2 \frac{\partial \rho}{\partial r} + g\rho = N_2, \tag{19}$$

where

$$N_1 = -\frac{1}{r^2}\frac{\partial}{\partial r}\left(r^2 \rho v_r\right), \tag{20}$$

$$N_2 = -\frac{\partial}{\partial t}(\rho v_r) - \frac{1}{r^2}\frac{\partial}{\partial r}\left(r^2 \rho_0 v_r^2\right) + \frac{4}{3}\eta_0 \frac{\partial}{\partial r}\left[\frac{1}{r^2}\frac{\partial}{\partial r}\left(r^2 v_r\right)\right]. \tag{21}$$

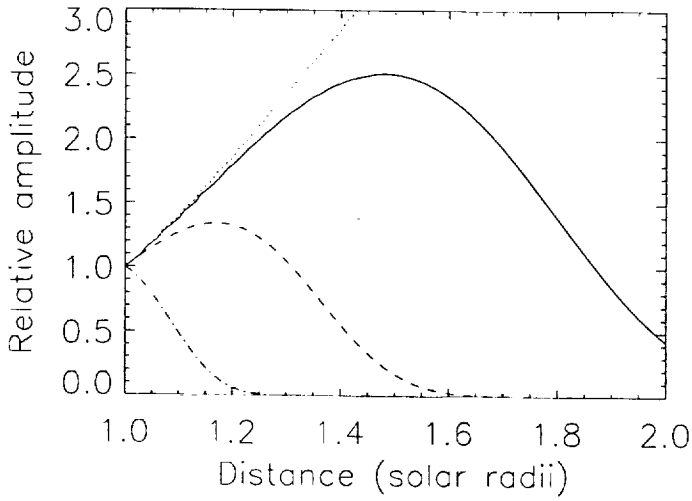

Fig. 1.— Dependence of the linear spherical slow wave amplitude on the distance from the Sun for four different normalized viscosities $\bar{\eta}$. The dotted line corresponds to $\bar{\eta} = 10^{-10}$, the solid line to $\bar{\eta} = 10^{-5}$, the dashed line to $\bar{\eta} = 10^{-4}$ and the dashed-dotted line to $\bar{\eta} = 10^{-3}$. The initial wave period is 600 s. The atmosphere is isothermal with $T = 1.4 \times 10^6$ K. The relative amplitude is given by $\bar{\rho}'(R)[\rho_0(R)\bar{\rho}'(1)]^{-1}$.

It is convenient to put dissipative terms on the right hand side as well.

Equations (18) and (19) can be combined into the weakly nonlinear wave equation

$$\frac{\partial^2 \rho}{\partial t^2} - \frac{C_s^2}{r^2}\frac{\partial}{\partial r}\left(r^2 \frac{\partial \rho}{\partial r}\right) - g\frac{\partial \rho}{\partial r} = \frac{\partial N_1}{\partial t} - \frac{1}{r^2}\frac{\partial}{\partial r}\left(r^2 N_2\right). \tag{22}$$

The right hand side terms N_1 and N_2 contain v_r, which can be expressed through ρ using the linear equation (10). Equation (22) becomes Equation (13) in the linear limit.

In the following, we consider the dynamics of the slow waves, assuming

$$\frac{\lambda}{H} \ll 1 \quad \text{and} \quad \frac{\eta_0}{C_s \rho_{00} \lambda} \ll 1, \tag{23}$$

where λ is the wavelength, in addition to assumption (17). Conditions (23) correspond to the WKB approximation and the approximation of weak dissipation, respectively. These approximations allow us to consider slow modification of the waves by the weak nonlinearity and dissipation in the WKB approximation. The latter means that we neglect the wave reflection from the radial inhomogeneity.

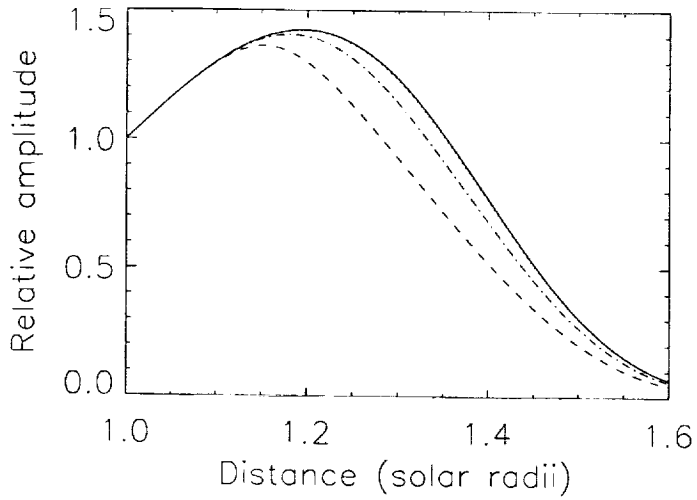

Fig. 2.— Dependence of the nonlinear spherical slow wave amplitude on the distance from the Sun for four different initial amplitudes $A = \rho(1)/rh_0(1)$. The solid line corresponds to $A = 10^{-6}$, the dotted line to $A = 0.02$, the dash-dotted line to $A = 0.08$ and the dashed line to $A = 0.16$. The initial wave period is 600 s. The atmosphere is isothermal with $T = 1.4 \times 10^6$ K. The normalized viscosity is $\bar{\eta} = 3.2 \times 10^{-4}$ (i.e., "typical solar value"). The relative amplitude is given by $\bar{\rho}'(R)[\rho_0(R)\bar{\rho}'(1)]^{-1}$.

Considering an outwardly propagating wave, we transform into the moving frame

$$\xi = r - C_s t, \qquad R = \epsilon r, \tag{24}$$

where the parameter ϵ is small, representing the *slow* modification of the wave by the *weak* nonlinearity, stratification and dissipation. This allows us to apply the standard method of slowly varying amplitudes. Keeping terms of the first order of ϵ only, we have from Eqs. (19), (20) and (21) we get

$$v_r = \frac{C_s}{\rho_0}\rho, \quad N_1 = -\frac{C_s}{\rho_0}\frac{\partial}{\partial\xi}\rho^2, \quad N_2 = \frac{4\eta_0 C_s}{3\rho_0}\frac{\partial^2\rho}{\partial\xi^2}, \tag{25}$$

and, finally, arriving at the evolutionary equation,

$$\frac{\partial\rho}{\partial R} + \left(\frac{1}{R} + \frac{g(R)}{2C_s^2}\right)\rho + \frac{1}{\rho_0(R)}\rho\frac{\partial\rho}{\partial\xi} - \frac{2\eta_0}{3C_s\rho_0(R)}\frac{\partial^2\rho}{\partial\xi^2} = 0. \tag{26}$$

Equation (26) is a spherical analog of the Burgers equation for slow magnetosonic waves. When all three factors of the wave evolution (the stratification, nonlinearity and dissipation)

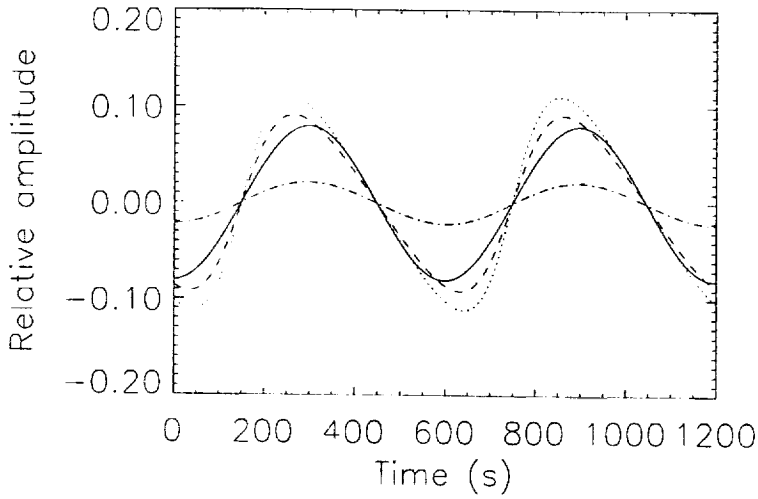

Fig. 3.— Evolution of temporal dependences of initially harmonical nonlinear spherical Alfvén waves with the distance from the Sun. The solid curve corresponds to the solution at $R' = 1R_\odot$, the dotted at $R' = 1.15R_\odot$, the dashed to $R' = 1.3R_\odot$ and the dash-dotted to $R' = 1.5R_\odot$. The initial wave amplitude is $A = 0.08$. The initial wave period is 600 s. The atmosphere is isothermal with $T = 1.4 \times 10^6$ K. The normalized viscosity is $\bar{\eta} = 3.2 \times 10^{-4}$. The relative amplitude is given by $\bar{\rho'}(R)/\rho_0(R)$.

modeled by the second, third and forth terms of Equation (26), respectively, are negligible, the wave form ρ is independent of R ($\rho(R) = \text{const}$). Consequently, the wave keeps its shape in the moving (with the speed C_s) frame of reference. When some of the evolution factors are taken into account, the wave form ρ depends on R, so the wave changes with the distance from the Sun.

For the following consideration, it is convenient to introduce the dimensionless variables

$$\xi' = \xi/R_\odot, \quad R' = R/R_\odot, \quad \rho' = \rho/\rho_{00}, \quad H' = H/R_\odot, \quad \rho'_0 = \rho_0/\rho_{00}, \tag{27}$$

where H is the scale height. With variables (27), equation (26) can be re-written as

$$\frac{\partial \rho'}{\partial R'} + \left(\frac{1}{R'} + \frac{1}{2H'R'^2}\right)\rho + \frac{1}{\rho_0(R')}\rho'\frac{\partial \rho'}{\partial \xi'} - \frac{\bar{\eta}}{\rho_0(R')}\frac{\partial^2 \rho'}{\partial \xi'^2} = 0, \tag{28}$$

where $\bar{\eta} = \frac{2}{3}\eta_0/C_s\rho_{00}R_\odot$.

When both nonlinearity and viscosity (the third and the forth terms) are negligible,

Equation (28) is easily integrated, giving us

$$\rho'(R') = \rho'(1)\frac{1}{R'}\ \exp\left[-\frac{1}{2H'}\left(1-\frac{1}{R'}\right)\right]. \tag{29}$$

The linear solution (29) resembles solution (6) for a harmonic wave, but Eq. (29) is valid for waves of arbitrary initial shape as long as they satisfy conditions (23).

Both the effects of stratification and viscosity can be taken into account for a harmonic wave

$$\rho(R', \xi') = \bar{\rho}'(R')\ \exp(ik\xi'), \tag{30}$$

where k is a dimensionless wave number. Substituting expression (30) into Equation (28) (where the third term, corresponding to nonlinearity, is neglected), we obtain

$$\bar{\rho}' = \rho'(1)\frac{1}{R'}\ \exp\left[-\frac{1}{2H'}\left(1-\frac{1}{R'}\right)\right]$$

$$\times \exp\left\{-\bar{\eta}k^2\int_1^{R'}\exp\left[\frac{1}{H'}\left(1-\frac{1}{R''}\right)dR''\right]\right\}. \tag{31}$$

Expressing the integral through the exponential integrals $\mathrm{Ei}(x)$, we have

$$\bar{\rho}'(R') = \rho'(1)\frac{1}{R'}\ \exp\left[-\frac{1}{2H'}\left(1-\frac{1}{R'}\right)\right]$$

$$\times \exp\left(\bar{\eta}k^2\left\{1 - R'\mathrm{e}^{\frac{1}{H'}\left(1-\frac{1}{R'}\right)} + \frac{1}{H'}\mathrm{e}^{\frac{1}{H'}}\left[\mathrm{Ei}\left(-\frac{1}{H'}\right) - \mathrm{Ei}\left(-\frac{1}{R'H'}\right)\right]\right\}\right). \tag{32}$$

Expression (32) shows that there are two different scenarios of the wave propagation. When $\bar{\eta}k^2$ is less than the critical value $(\bar{\eta}k^2)_c$, the relative amplitude of the wave, $\bar{\rho}'/\rho_0$ initially grows, reaches a maximum, and then decays. For $\bar{\eta}k^2 > (\bar{\eta}k^2)_c$, the wave decays from the very beginning. Dependence of the wave amplitude on distance from the Sun for different values of the viscosity are shown in Figure 1. The dotted curve corresponds to the dissipationless solution (29). When the medium has finite viscosity, the wave either reaches a maximum and then decays or decays from $R' = 1R_\odot$. To determine the critical value of the viscosity $(\bar{\eta}k^2)_c$, we expand the function $\bar{\rho}'/\rho_0$ into a Taylor series near $R' = 1$:

$$\bar{\rho}'/\rho_0 \sim 1 + \left(\frac{1}{2H'} - 1 - \bar{\eta}k^2\right)(R' - 1). \tag{33}$$

From the condition that the coefficient with $R' - 1$ changes sign, we obtain

$$(\bar{\eta}k^2)_c = \frac{1}{2H'} - 1. \tag{34}$$

For a given viscosity, waves with wavelengths shorter than

$$\lambda < 2\pi\sqrt{\frac{2H'\bar{\eta}}{1-2H'}} \tag{35}$$

are decaying at $R' = 1R_\odot$. For a given wave period P, waves are decaying at $R' = 1R_\odot$ for viscosities higher than

$$\bar{\eta} > \left(\frac{C_s P}{2\pi R_\odot}\right)^2 \left(\frac{1}{2H'} - 1\right). \tag{36}$$

Consequently, only sufficiently long wavelength slow waves are propagating along plumes. However, if the relative wave amplitude grows with the distance from the Sun, nonlinear effects, described by the third term in Equation (28), come into play. The nonlinear generation of higher harmonics transfers the wave energy into the short wavelength part of the spectrum, where the strong dissipation takes place. Thus, waves of higher amplitude are subject to stronger dissipation. This is shown in Figures 2 and 3. Figure 2 shows the growth of the wave amplitude for three different initial amplitudes. (The curves are normalized on the initial amplitudes). The waves of higher amplitudes reach their maxima quicker. In the vicinity of the maximum, the wave amplitude decays due to nonlinear dissipation. Nonlinear evolution of the wave shape is shown in Figure 3. Initially, the outward propagating wave grows and its shape steepens departing from a simple harmonic shape. Finally, as the wave propagates outward, its amplitude decreases and the waves returns to the initial harmonic shape.

The analytical theory allows us to understand main features of short wavelength dynamics of slow magnetosonic waves in the radially stratified static atmosphere, taking into account effects of *weak* nonlinearity and dissipation. However, the analytical theory is based upon assumptions (17) and (23). In particular, the assumption that the wavelength is much less than the scale height, is not well justified for modeling of the slow waves in polar plumes. Also, effects of two-dimensional structuring as well as radial plasma flows, which affects the waves, are out of scopes of the analytical theory. Thus, in in the next section we present the results of more realistic quantitative modeling of the waves using the nonlinear dissipative 1D, and 2D MHD model.

2.1.4. 2D MHD Results

The purpose of the 2D MHD simulations is to investigate the effects of the plume density and temperature structure on the propagation and the dissipation of the slow magnetosonic waves. The 2D MHD simulations are initiated with the normalized number density and temperature profiles that represent a polar plume

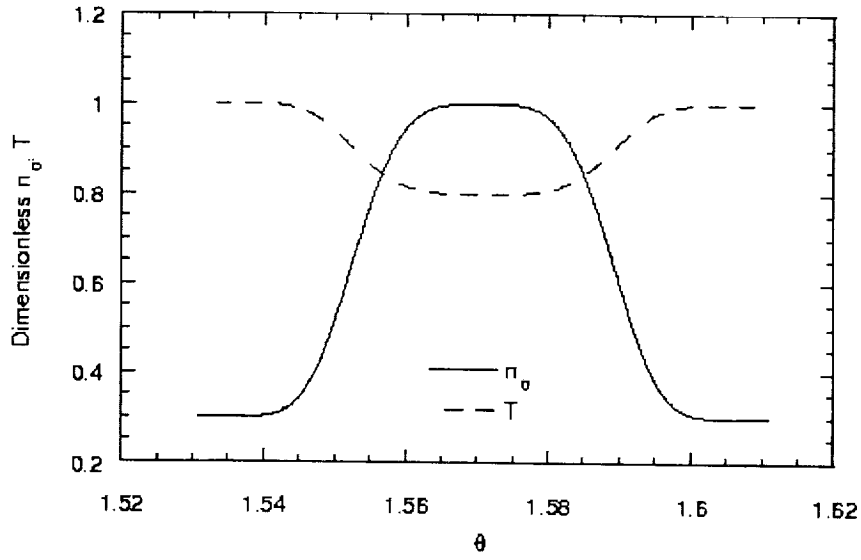

Fig. 4.— The θ-dependence of the initial normalized density and temperature of the plume.

$$n_0(\theta, r) = \left[n_{\min} + (1 - n_{\min})\, e^{-[(\theta-\pi/2)/d]^4}\right] n_0(r), \tag{37}$$

$$T(\theta, r) = T_{\max} - (T_{\max} - T_{\min})\, e^{-[(\theta-\pi/2)/d]^4} \tag{38}$$

where the angular plume half-width $d = 0.04$ Rad, and the normalized density of the surrounding coronal hole $n_{\min} = 0.3$, with the normalization $n_0(1) = 1$ at the center of the plume. The normalized temperature in the center of the plume $T_{\min} = 0.8$ is lower than the normalized temperature of the surrounding corona $T_{\max} = 1$. The θ dependence of n_0 and T is shown in Fig. 4. In the uniform magnetic field, such structure is a waveguide for trapped fast and slow magnetosonic waves. The initial radial dependence of v_r and n_0 is given by Parker's (1963) isothermal solar wind solution.

The initial magnetic field $\mathbf{B} = B_0(r)\mathbf{e}_r$ is uniform in the θ-direction and varies as $\frac{1}{r^2}$. We use the following typical coronal hole parameters in our 2D run $n_{00} = 5 \times 10^8$ cm^{-3}, $B_0 = 10$ G, $v_A = 975$ km s^{-1}, $C_s = 152$ km s^{-1}, $\tau_A = 718$ s, and we set $S = 10^6$, $\eta_0 = 5 \times 10^{-5}$, and $T = 1.4 \times 10^6 K$.

For the upper boundary of the plumes and at the θ-boundaries we use open boundary conditions. We allow for incoming characteristics at the solar boundary by using zero-order extrapolation for the variables (e.g., Steinolfson & Nakagawa 1976). The density perturbation $n_1(\theta, r = 1, t)$ is driven harmonically with the frequency $\omega = 7.5$ and an

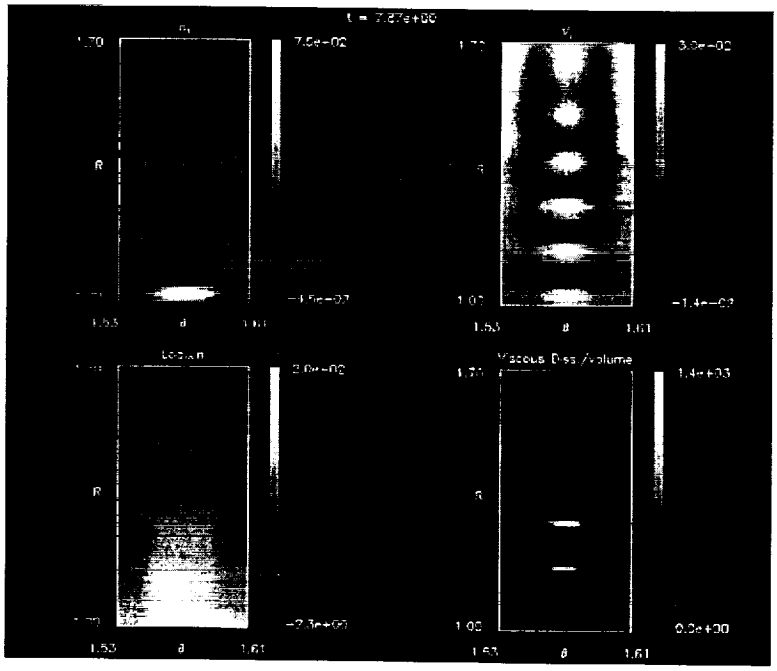

Fig. 5.— A snapshot at $t = 8.55\tau_A = 102.2$ min of the spatial variations of the perturbed density n_1, v_r, n, and S_v due to the propagating slow magnetosonic wave in the model polar plume.

amplitude of $n_d = 0.08$:

$$n_1(\theta, r = 1, t) = n_d\, e^{-[(\theta-\pi/2)/d]^2} sin\, \omega t. \tag{39}$$

The magnetosonic waves that are excited with the above driver are not coupled to Alfvénic fluctuations since $\partial/\partial\phi = 0$. Thus v_ϕ and B_ϕ remain zero throughout the simulation in the plume. The slow wave is coupled to v_θ and B_θ. However, the perturbations in v_θ and B_θ remain small in our runs.

We solve the 2D MHD equations using the fourth order Runge-Kutta method for temporal integration and fourth order spatial differencing with 600 grid points in the radial direction and 40 grid points across the half-width of the plume. We use symmetry boundary conditions at the center of the plume. In Figure 5 the spatial variations in the perturbed density n_1, v_r, n, and S_v at $t = 8.55\tau_A = 102.2$ min are shown.

The spatial variation in n_1 and v_r are nearly in phase, as expected from the linear theory of traveling waves in a dissipative medium. It is evident that the plume width affects the shape of the waves and leads to trapping of the waves. However, small amplitude magnetosonic waves can be detected outside the plume. This could be due to the energy contained in the tails of the Gaussian shape driver (Eq. (39)), small leakage of the wave

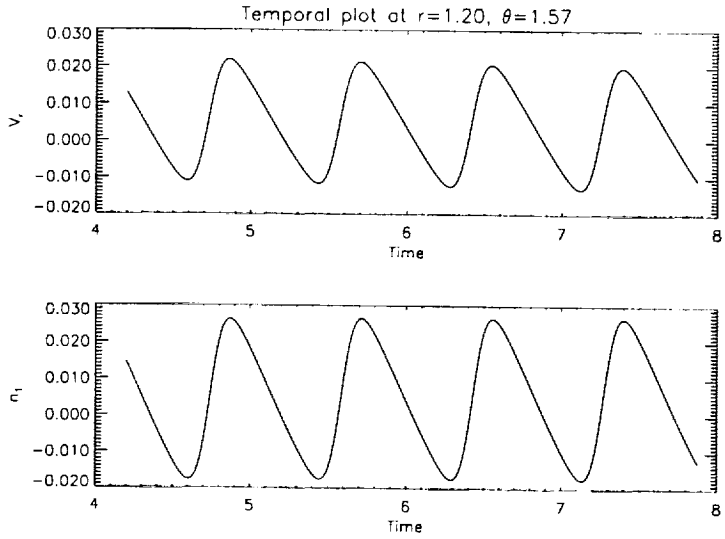

Fig. 6.— The temporal variations of n_1 and v_r in the plume at $r = 1.20$ and $\theta = 1.57$ due to the propagating magnetosonic wave.

energy outside the plume, or evanescent tails of the trapped modes. The lower temperature inside the plume compared to the surrounding corona results in lower sound speed there. This leads to the bending of the wave fronts, and the corresponding bending of the viscous dissipation layers.

The amplitude of the waves is small ($n_1/n_0 \ll 1$), and the solution is nearly linear near the solar surface. As the magnetosonic waves propagate outwards, the quantity n_1/n_0 increases and the nonlinear steepening of the waves becomes apparent. The steepening of the waves is limited by the presence of the viscous dissipation, and no shocks can be formed. However, the sharper gradients near the wave fronts lead to enhanced viscous dissipation there. The heating is distributed along the plume by the propagating waves up to a distance determined by the dissipation length of the waves.

In Figure 6 we show the temporal variation of v_r, and n_1 at $r = 1.20R_\odot$ and $\theta = 1.57$ (i.e., near the central axis of the plume). It is evident that the modeled density and velocity fluctuations of the traveling waves are in phase, as expected from the linear theory. The nonlinear steepening of the wave fronts and the resulting asymmetry in the shape of the waves is evident in the temporal evolution. The steepening is limited by the presence of compressive viscosity. Nonlinearity also modifies the initial hydrostatic background equilibrium and leads to changes in the wave amplitude and phase speed with time.

The effects of nonradial plume divergence on the propagation and the dissipation of

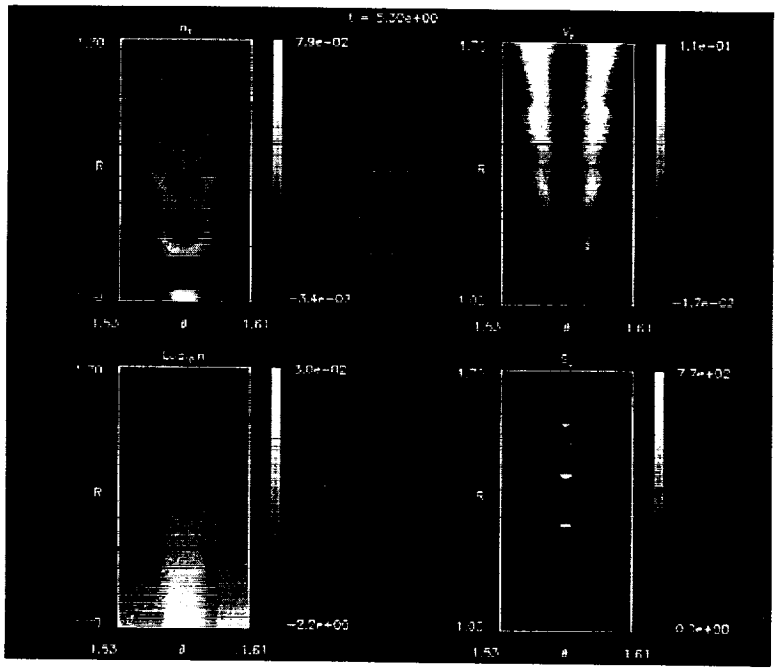

Fig. 7.— A snapshot at $t = 5.30\tau_A = 63.4$ min of the spatial variations of the perturbed density n_1, v_r, n, and S_v due to the propagating slow magnetosonic wave in the nonradial model polar plume with $d = 0.01$ at $r = 1R_\odot$.

the slow magnetosonic waves are investigated by adding a quadrupole component to the radial background field:

$$\mathbf{B} = \left[\frac{B_0}{r^2} - \frac{3B_4(3\cos^2\theta - 1)}{2r^4}\right]\mathbf{e}_r - \frac{3B_4 \sin 2\theta}{2r^4}\mathbf{e}_\theta, \tag{40}$$

where we set $B_0 = 0.1$ and $B_4 = 0.6$ to get and B(1,π/2)=1 and an asymptotic divergence rate of 10. At $r = 2R_\odot$ the cross sectional area of the plume diverged by a factor of about 3. At $r = 1R_\odot$ we set $d = 0.01$, and we model this divergence rate in the density structure of the plume by substituting $d \rightarrow d(r) = d(1)\, B_r(r, \pi/2)^{1/2} r$ in Equations (37)-(38). B_θ, and the θ dependence of B_r is neglected in the divergence factor due to the small angular extent of the plume. The initial radial dependence of the density is taken to be locally hydrostatic with the temperature $T(r, \theta)$. The initial state evolves to a self consistent solution during the 2D simulation.

The spatial dependence of the solutions for the nonradial plume is shown in Figure 7 with $n_0 = 5 \times 10^8$, $\omega = 7.5$, $T(\theta = \pi/2) = 1.12 \times 10^6$ K. The faster-than-radial expansion of the plume is evident in the spatial structure of the density. The main difference between

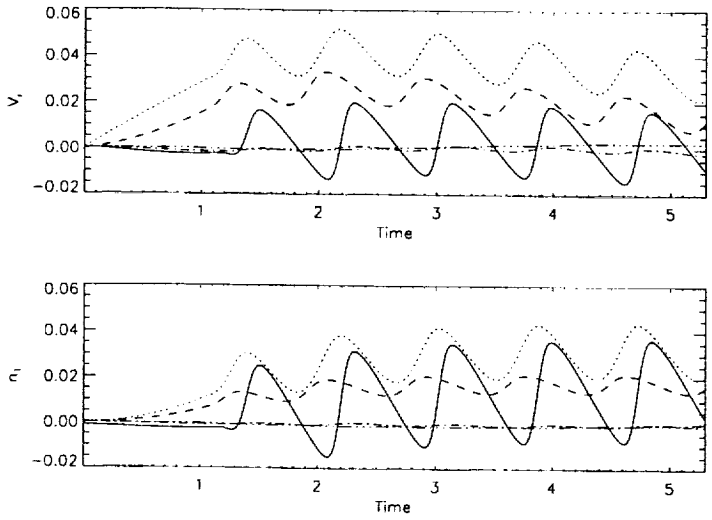

Fig. 8.— The temporal variations of n_1 and v_r in the plume at $r = 1.20$ and $\theta = 1.57$ (solid), $\theta = 1.58$ (dotted), $\theta = 1.59$ (dashed), $\theta = 1.60$ (dash-dot), $\theta = 1.61$ (dash-dot-dot-dot) due to the propagating magnetosonic wave for the case in Figure 7.

the radial and the nonradially divergent plume is in the morphology of the wave, S_v, and the v_r. The perturbations of the density are excited at the base of the plume and expand across the plume as they propagate upward. The density fluctuations are in phase with velocity fluctuations. The enhanced radial velocity of at the edges of the plume is due to the increase pressure gradient at the plume boundary. The viscous dissipation of the waves is more concentrated at the center of plume than in the radial case.

The temporal evolution at $r = 1.2R_\odot$ at several locations across the plume and the coronal hole are shown in Figure 8. It is evident that the phase speed, and the amplitude of the waves varies considerably across the plume. At $r = 1.2R_\odot$ initial state evolves to a self-consistent solution within about $1.5\tau_h$. The long term variations are due to the nonlinear evolution of the density and velocity in the plume and the surrounding coronal hole.

2.2. Two Fluid Coronal Hole Model

Neglecting electron inertia ($m_e \ll m_p$; $\mathbf{V} = \mathbf{V}_p$; $\rho = m_p n$), and relativistic effects ($V \ll c$), assuming quasi-neutrality ($n = n_e = n_p$), neglecting minor ions, we get the 2-fluid

MHD equations

$$\frac{\partial \rho}{\partial t} + \nabla \cdot (\rho \mathbf{V}) = 0, \tag{41}$$

$$\rho \left[\frac{\partial \mathbf{V}}{\partial t} + (\mathbf{V} \cdot \nabla)\mathbf{V} \right] = -(\nabla p_e + \nabla p_p) - \frac{GM_\odot \rho}{r^2} + \frac{1}{c}\mathbf{J} \times \mathbf{B} - \nabla \cdot \Pi, \tag{42}$$

$$\frac{\partial \mathbf{B}}{\partial t} = -c\nabla \times \mathbf{E}, \quad \mathbf{E} = -\frac{1}{c}\mathbf{V} \times \mathbf{B} + \eta \mathbf{J} + \frac{1}{n\,e\,c}\mathbf{J} \times \mathbf{B} - \frac{\nabla p_e}{n\,e}, \tag{43}$$

$$\nabla \times \mathbf{B} = \frac{4\pi}{c}\mathbf{J}, \qquad \mathbf{V}_e = \mathbf{V} - \frac{\mathbf{J}}{n\,e}, \tag{44}$$

$$\frac{\partial p_p}{\partial t} = -\gamma_p p_p \nabla \cdot \mathbf{V} - \mathbf{V} \cdot \nabla p_p + S_v, \; \frac{\partial p_e}{\partial t} = -\gamma_e p_e \nabla \cdot \mathbf{V}_e - \mathbf{V}_e \cdot \nabla p_e + S_e, \tag{45}$$

In the above equations we use the following normalization: $r \rightarrow r/R_s$; $t \rightarrow t/\tau_A$; $V \rightarrow V/V_A$; $B \rightarrow B/B_0$; $\rho \rightarrow \rho/\rho_0$; $p_p \rightarrow p_p/p_{p0}$; $p_e \rightarrow p_e/p_{e0}$. $S = \tau_r/\tau_A$ the Lundquist number, $\tau_r = 4\pi a^2/\nu c^2$ the resistive time scale, $\tau_A = a/V_A$ the Alfvén time scale. In coronal holes for the relevant scales of $O(0.01 - 1R_\odot)$ the Hall term and the electron pressure terms are small in the Ohm's law compared to the other terms, and $\mathbf{V}_p \approx \mathbf{V}_e$. The Ohmic heating term in the electron energy equation is $S_e = (\gamma_e - 1)j^2/S$, Pi is the viscous stress tensor, and S_v is the viscous ion heating term.

To model the effect of random disturbances on the generation of waves we use a broad-band Alfvén wave source at $r = 1R_\odot$ given by

$$B_\phi(t, \theta, r = 1) = -V_d/V_{A,r} F(t, \theta) \tag{46}$$

$$F(t, \theta) = \sum_{i=1}^{100} a_i sin(\omega_i t + \Gamma_i(\theta)) \tag{47}$$

where $a_i = a_0 i^{-1/4}$, $a_0 = 0.115$, $\omega_i = \omega_1 + (i-1)\Delta\omega$, $\Delta\omega = (\omega_N - \omega_1)/(N-1)$, and Γ_i is a random phase. We use frequencies in the range of 1.4-6.9 mHz.

2.2.1. Results of the 2-fluid Model

In Figures 9-13 we show the results of the two-fluid run with the physical parameters $\gamma_p = 1.1$, $\gamma_e = 1.05$, $T_{p0} = 2 \times 10^6$ K, $T_{e0} = 0.8 \times 10^6$ K, $n_0 = 10^8$ cm^{-3}, $B_0 = 7$ G, $V_A = 1527$ km/s, $V_d = 0.06$. The Lundquist number is set to $S = 10^4$.

The spatial dependence of the velocity components and the density at $t = 130\tau_A = 16.5$ hrs are shown in Figure 9. The Alfvénic velocity component v_ϕ (bottom right panel) fluctuates out-of-phase with B_ϕ (see Figure 10) as the waves propagate in the coronal hole.

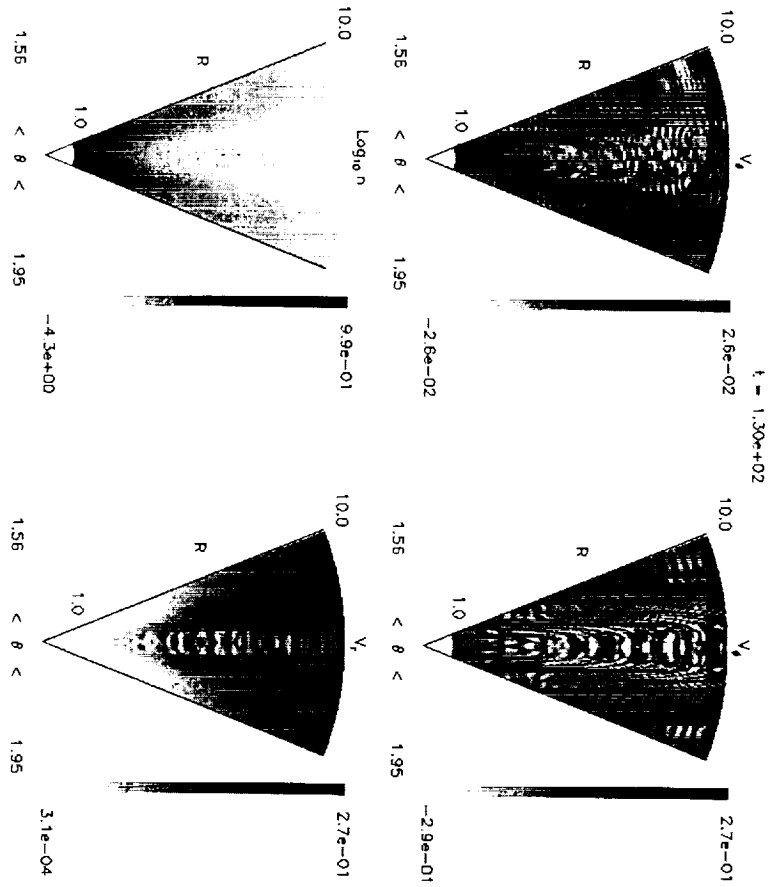

Fig. 9.— The spatial dependence of the density and the velocities in the model coronal hole at $t = 130\tau_A = 16.5$ hrs.

The fluctuations in v_ϕ were used to calculated the effective proton temperature discussed below. The v_r (bottom left panel) reached about 400 km/s near $r = 10R_\odot$ and has not approached the asymptotic speed in this region. The fluctuations in v_r in the central region of the coronal hole are due to the nonlinear compressional waves driven by Alfvén waves. The v_θ remains small throughout the coronal hole. We have used the linearly polarized Alfvén waves as the driver at the coronal boundary. Including other polarizations may produce larger v_θ.

In Figure 10 we show the corresponding magnetic field components and j^2/ρ (proportional to the Ohmic heating per particle). It is evident that the largest gradients in B_ϕ occur at the boundaries of the coronal hole, defined by the transition from low to

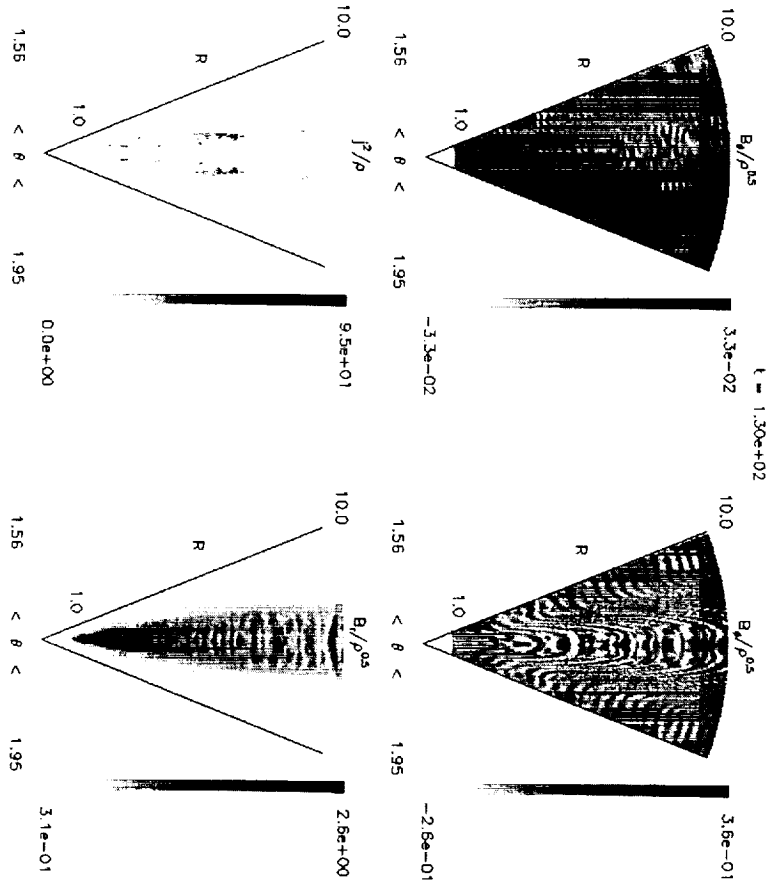

Fig. 10.— The spatial dependence of the magnetic field components and j^2/ρ in the model coronal hole at $t = 130\tau_A = 16.5$ hrs.

high density regions. The phase-mixing of the Alfvénic wave fronts leads to the generation of currents (see, also in this issue). The large currents in these regions lead to heating of the electrons via Ohmic dissipation, which is evident in the electron temperature (see Figure 11) below. The fluctuations in B_θ are small compared to B_ϕ in accordance with the small fluctuations in v_θ. The variations in $B_r/\rho^{0.5}$ are due to the effects of the nonlinear compressional waves.

The 2D distribution of the electron temperature in the model coronal hole is shown in the left panel in Figure 11. The electron temperature decreases from 0.8×10^6 K at the base of the corona to about 0.6×10^6 K at $10R_\odot$. Two regions of somewhat higher electron temperature are evident in the model coronal hole in the boundary between the low and

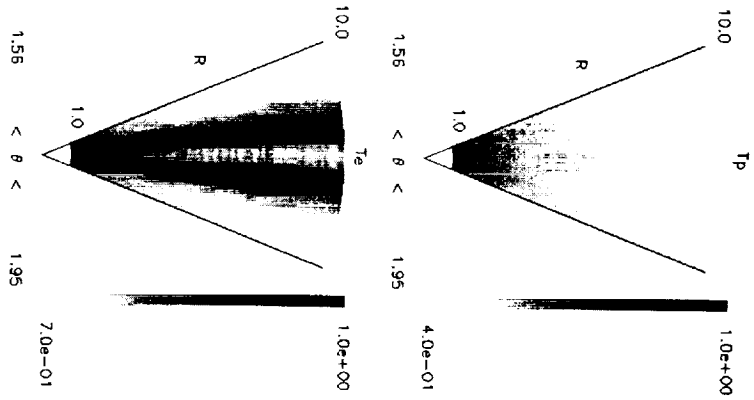

Fig. 11.— The spatial dependence of the electron and proton temperatures in the model coronal hole at $t = 130\tau_A = 16.5$ hrs.

the high density regions. The higher temperature is the result of the Ohmic heating due to phase-mixing of the Alfvén waves in the inhomogeneous regions (see j^2/ρ in Figure 10). The proton temperature (right panel) is not affected by the Ohmic heating and decreases nearly monotonically from 2×10^6 K at $r = 1R_\odot$ to 0.9×10^6 at $10R_\odot$.

The radial dependence of the electron and proton temperatures and of v_ϕ and v_r are shown in Figure 12. The fluctuations due to the nonlinear waves driven by the Alfvén waves are evident in the v_r, T_p, and T_e. The nonlinear waves contribute to the acceleration of the solar wind in addition to the thermal gradient.

In Figure 13 we show the temporal evolution of the velocity components (top panel) and the density perturbation (bottom panel) at $r = 4.98R_\odot$ at the center of the coronal hole. It is evident that the fluctuations due to the nonlinear waves in v_r and ρ_1 are in phase as would be expected for compressional longitudinal wave. The Alfvénic fluctuations of the v_ϕ are dominated by higher frequency than the nonlinear compressional wave.

In Figure 14 we show the effect of v_ϕ on the line-width temperature. The dashed line shows the time-averaged proton temperature obtained form the model. This temperature is decreasing as expected from the Polytropic energy equation. The solid line shows the effective line-width temperature that incorporates the effect of waves on the simulated line width. The effective temperature calculated using $T_{p,eff} = T_p + \frac{m_p}{2k_b} < V_\perp^2 >$, is due to unresolved wave motions integrated over the line of sight in space and about 4 hours in time. It is evident that the effective line-width temperature increases with r in qualitative agreement with SOHO UVCS Ly-α observations Kohl et al. 1998. In the period covered by

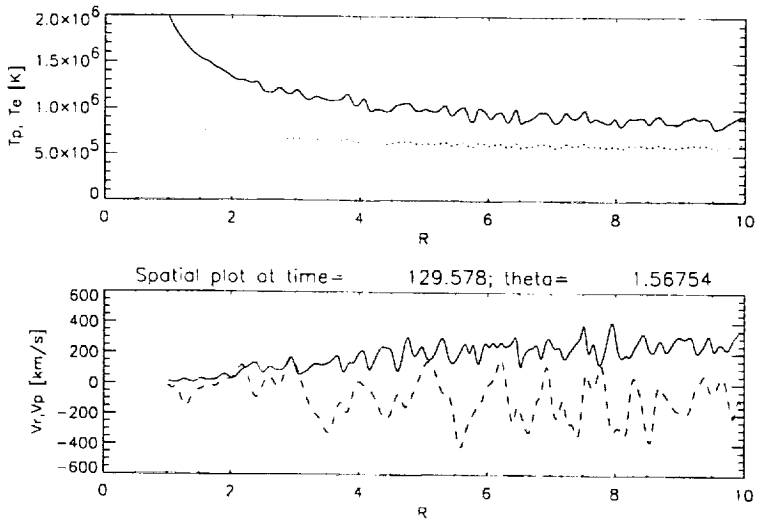

Fig. 12.— The radial dependence of T_p (solid line) and T_e (dashed line) at the center of the model coronal hole are shown in the top panel. The v_r (solid line) and the v_ϕ (dashed line) are shown in the bottom panel.

this report we have further explored the parameter space of the solar wind with the 2.5-D two-fluid model. We have including the effects of self-consistent heating of the electrons by Ohmic dissipation, and heating of protons by viscous dissipation. We found that with millihertz range Alfvén waves the solar wind will be heated beyond several solar radii, provide that strong phase mixing of the Alfvén waves is present.

3. Analysis

Motivated by recent observations of slow magnetosonic waves in polar plumes by the EIT we investigated the propagation, and the dissipation of these waves. We derived the linear dispersion relation for these waves in the viscous plume plasma, and spherical geometry. We included the effects of weak quadratic nonlinearity and derived an evolutionary Burgers' type equation for these waves with the main assumptions of weak nonlinearity, short wavelength (compared to the scale height), and no background solar wind flow. Numerical solution of the evolutionary equations show the dependence of the wave amplitude with height. To relax the above assumptions we used the 1D and the 2D MHD equations to model the propagation, and the dissipation of the slow waves in plumes. The MHD models included compressive viscosity, self-consistent nonlinear effects, and background solar wind flow. The results of the simulations describe the dynamics and the

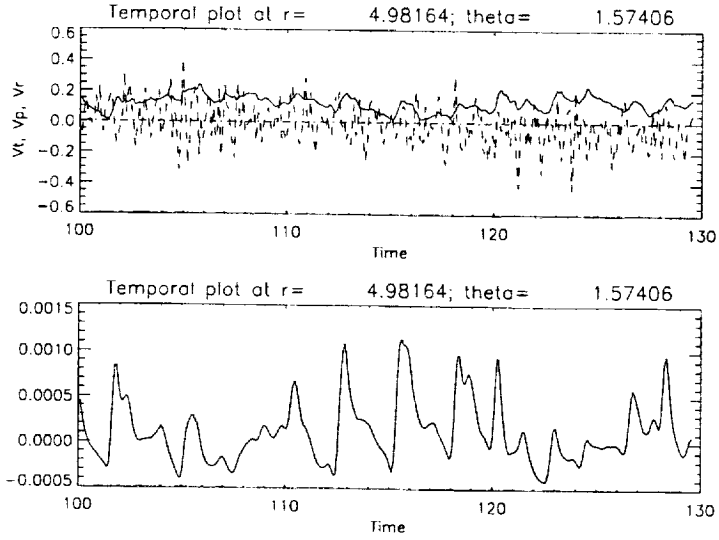

Fig. 13.— The temporal evolution of v_r (solid line, top panel), v_ϕ (dashed line, top panel) and the perturbed density (bottom panel) in the center of the coronal hole.

dissipation of the waves for a range of coronal parameters.

The required energy flux to heat the corona (i.e., to balance the radiative and conductive losses) is about 10^5 ergs cm^{-2} s^{-1}. The energy flux carried by the slow magnetosonic waves is given by $\rho\frac{(\delta v)^2}{2}C_s$ in the WKB approximation. For $n = 5 \times 10^8$ cm^{-3} and $T = 1.4 \times 10^6$ K, the required wave amplitude to obtain sufficient energy flux to balance the losses is 40 km s^{-1}. This wave amplitude is consistent with the observed nonthermal broadening of emission lines (e.g, Chae, Schuhle, & Lemaire 1998). The direct observation of slow magnetosonic waves in coronal plumes by DeForest and Gurman (1998) using the EIT instrument shows that these waves are present in coronal hole plumes.

Slow magnetosonic waves with an amplitude of 40 km s^{-1} (about 27% of the sound speed) carry an order of magnitude more energy than the $\sim$15 km s^{-1} that were seen in EIT observations. The 40 km s^{-1} waves are in the nonlinear regime with significantly shorter dissipation length than the length predicted by the linear theory. We found numerically that due to nonlinear steepening of the wave fronts the dissipation length near the Sun is about $0.08R_\odot$ for these waves, compared to $0.14R_\odot$ for the 15 km s^{-1} waves with 300 s period and solar value of compressive viscosity.

The short dissipation length of high amplitude five-minute slow magnetosonic waves will make them hard to detect by the EIT instrument, since the signal would be dominated by the longer period, smaller amplitude waves that have longer dissipation length. In

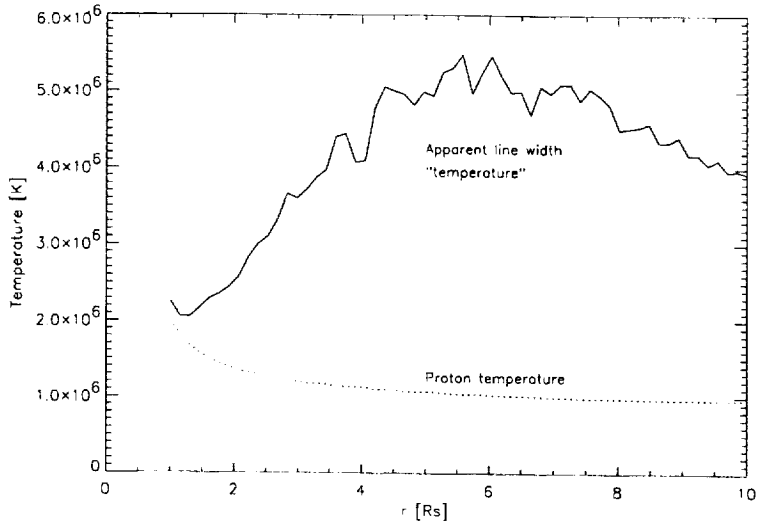

Fig. 14.— Effective (i.e., including the effect of waves) and model line-of-sight time-averaged proton temperatures.

addition, the available cadence of EIT does not allow observations of waves with periods below ~6 minutes. The UVCS WLC observations at $1.9R_\odot$ reported by Ofman et al. (1997, 1998) are at higher cadence of $\sim$ 90 s. Our simulations show that most of the waves in the millihertz frequency range would be dissipated by $1.9R_\odot$ for solar value of the compressive viscosity with $T = 1.4 \times 10^6$ K. The detection of these waves at $1.9R_\odot$ possibly indicate that the effects of compressive viscosity are somewhat lower allowing the slow wave to propagate to $1.9R_\odot$. This could be due to somewhat lower temperature, or higher density than the values used as "typical" solar values in our study. It is also possible that the slow waves are generated locally above $1R_\odot$.

We extended OD model by using more realistic parameters and source terms in the MHD equations. We improved the numerical technique and geometry of OD, replacing the hydrostatic initial state with Parker's (1963) isothermal solar wind solution and with more complex initial magnetic field, and source terms. In particular, we found that the low frequency Alfvén waves with a period of about an hour drive LAN waves in the radial flow velocity, which contributes significantly to the acceleration of the solar wind in coronal holes such that the fluctuating solar wind speed at $32R_\odot$ agrees with the observed fast solar wind speed of $500 - 900$ km s^{-1} (Grall et al. 1996). We found that in order to heat the solar wind to 10^6 K we need to deposit the heating close to the Sun by including strong phase mixing in solar wind inhomogeneities. We found that the dynamical evolution and the spatial variability of the LAN wave driven wind are in better qualitative agreement

with observations than the slowly varying, thermally driven and WKB Alfvén wave solar wind models (for a review of recent models and observations see Winterhalter et al. 1996).

We included a broad-band spectrum of the Alfvén waves and investigated the effect of two-temperature electron-ion plasma of the solar wind on the signatures of the waves that would be expected from the SOHO UVCS observations. For this purpose we have solved the two-fluid MHD equations and found that the effective proton temperature in the model increases with height. The extension of our model into the two-fluid description with a broad band Alfvén wave source and more realistic heating terms enables us to include more realistic electron and proton temperatures.

The SOHO/UVCS observations suggest that $T_p > T_e$ in coronal holes. We use the two-fluid 2.5D MHD model to investigate the self-consistent acceleration and heating of the two-temperature electron-proton plasma by a broad band Alfvén wave source. We calculate the effective line-width proton temperature using the results of the 2.5D two-fluid model, an increase of the line-width proton temperature with heliocentric distance. This effect is in qualitative agreement with UVCS observations of the increase of the Ly-α line width with height.

Our coronal hole model suggest that the observed increase of the line-width proton temperature is due to temporally and spatially unresolved low-frequency wave motions of the protons. Thus, the MHD waves may contain a significant fraction of the solar wind energy in the lower corona, and therefore, may play an important role in the acceleration and heating of the fast solar wind.

4. Recommended further action

We plan to improve the energy equation in our model by relaxing the polytropic assumption and to investigate the effects of a realistic heat conduction term. Due to the small time step required to correctly describe the thermal conduction with an explicit numerical method we are able to include the heat conduction terms in the 1D version of our 2D code. In order to eliminate this limitation and use the full 2D capabilities of our code we plan to use an implicit method for the energy equation. This will allow to include the heating terms due to waves more realistically in our model. We will also plan to extend the plume study to the multi-fluid model with the more realistic energy equations for proton and electrons, and with self consistent heating terms. We plan to further improve the execution speed of our code by continue the optimization for parallel execution on the Cray T3E.

In the third year of this project we plan to expand our model in two ways: (1) we plan to include a second ion fluid in the equations, and thus to develop a three-fluid model. This is needed in order to understand recent SOHO/UVCS observations of the solar corona in Oxygen emission at 1032Å and in other minor ion emission; (2) we plan to expand our model into a full 3D description, which will allow to use more realistic model of a coronal hole and solar boundary conditions. For this purpose we will include the $\partial/\partial\phi$ terms in our single fluid model, and investigate various methods of solutions, and the effect of boundary conditions. Initially, we will develop the code on our SGI workstations. Next, we will investigate the timing and the efficiency of the solution on the Cray J90 and the Cray T3E.

5. Publications

Below is the list of publications that were supported in full or in part by this contract in the period covered by the report.

1. Ofman, L., Davila, J.M., Two-fluid 2.5D MHD Model of the Fast Solar Wind and the Effective Proton Temperature, in Solar Wind Nine, S. Habbal et al. (eds), AIP Conference Proceedings, 471. pp. 405-408, AIP, New York, 1999.

2. Davila, J.M., Ofman, L., Two-fluid 2.5D MHD Simulations of the Fast Solar Wind in Coronal Holes and the Relation to UVCS Observations, Space Science Review, Kluwer, *87*, 165, 1999.

3. Ofman, L., Dissipation and Steepening of Slow Magnetosonic Waves in Polar Plumes and the Effect on the Solar Wind Close to the Sun, Proceedings of the 8th SOHO Workshop, Plasma Dynamics and Diagnostics in the Solar Transition Region and Corona, ESA SP-446, pp. 515-518, ESTEC, Noordwijk, 1999.

4. Nakariakov, V.M., Ofman, L., DeLuca, E., Roberts, B., Davila, J.M., TRACE Observation of Damped Coronal Loop Oscillations: Implications for Coronal Heating, Science, *285*, 862, 1999.

5. V.M. Nakariakov, Ofman, L., T.D. Arber, Nonlinear Dissipative Spherical Alfvén Waves in Solar Coronal Holes, Astronomy and Astrophysics, *353*, 729, 2000.

6. Airapetian, V.S., Ofman, L., Robinson, R.D., Carpenter, K.G., Davila, J.M., Two-Component Winds from Luminous Late-type Stars, The Astrophysical Journal, 2000, in press.

7. Ofman, L., V. Nakariakov, N. Sehgal, Dissipation of Slow Magnetosonic Waves in Coronal Plumes, The Astrophysical Journal, 2000, in press.

REFERENCES

Alazraki, G., & Courtier, P. 1971, A&A, 13, 380

Athay, R.G., & White, O.R. 1979, ApJS, 39,333

Belcher, J.W. 1971, ApJ, 168, 509

Boynton G.C., and Torkelsson, U., 1996, Astron. Astrophys., 308, 299

Braginskii, S. I. 1965, Rev. Plasma Phys., 1, 205

Chae, J., Schühle, U., Lemaire, P. 1998, ApJ, 505, 957

Davila, J.M. 1985, ApJ, 291, 328

Davila, J.M. 1987, ApJ, 317, 514

DeForest, C.E., and J.B. Gurman 1998, ApJ, 501, L217

Esser, R., Habbal, S.R., Coles, W.A., Hollweg, J.V., 1997, J. Geophys. Res., 102, 7063

Hollweg, J.V. 1973, ApJ, 181, 547

Grall, R.R., Coles, W.A., Klinglesmith, M.T., Breen, A.R., Williams, P.J.S., 1996, Nature, 379, 429

Jacques, S.A. 1977, ApJ, 215, 942

Kohl et al.: 1998, *Astrophys. J*, **501**, 127

Lau, Y.-T., Siregar, E., 1996, Astrophys. J., 464, 1054

Lou, Y.-Q., 1993, J. Geophys. Res., 98, 3563

Ofman, L., Davila, J.M., Steinolfson, R.S. 1994, 421, 360

Ofman, L., & Davila, J.M. 1995, J. Geophys. Res., 100, 23413

Ofman, L., & Davila, J.M., 1997a, Astrophys. J., 476, 357

Ofman, L., & Davila, J.M., 1997b, Astrophys. J., 476, L51

Ofman, L., Davila, J.M., 1998, 103, 23677.

Ofman, L., Romoli, M., Poletto, G., Noci G., Kohl, J.L. 1997, ApJ, 491, L111

Ofman, L., Romoli, M., Poletto, G., Noci G., Kohl, J.L. 1998, ApJ, 507, L189

Ofman, L., Nakariakov, V., DeForest, C.E. 1999, ApJ, 514, 441

Ong, K.K., Musielak, Z.E., Rosner, R., Suess, S.T., Sulkanen, M.E., 1997, Astrophys. J., 474, L143

Parker, E.N. 1963, Interplanetary Dynamical Processes, New York, Interscience

Porter, L., Klimchuk, J.A., & Sturock, P.A. 1994, ApJ, 435, 482

Steinolfson, R.S., & Nakagawa, Y. 1976, ApJ, 207, 300

Torkelsson U., & Boynton G.C. 1998, MNRAS, 295, 55

Warren, H.P., Mariska, J.T., Wilhelm, K., Lemaire, P. 1997, ApJ, 487, L91

Winterhalter, D., Gosling, J.T., Habbal, S.R., Kurth, W.S., Neugebauer, M., Solar Wind Eight, AIP Conference Proceedings 382, AIP Press, Woodbury, New York, 1996.

NASA REPORT DOCUMENTATION PAGE (IN LIEU OF NASA FORM SF 298)

1. REPORT NO.	2. GOVERNMENT ACCESSION NO.	3. RECIPIENT'S CATALOG NO.

4. TITLE AND SUBTITLE Acceleration of the Fast Solar Wind by Solitary Waves in Coronal Holes	5. REPORT DATE CODE:

7. AUTHOR(S) Dr. Leon Ofman	8. PERFORMING ORGANIZATION REPORT NO:

9. PERFORMING ORGANIZATION NAME AND ADDRESS Raytheon STX Corporation 4400 Forbes Blvd. Lanham, MD 20706	10. WORK UNIT NO. 11. CONTRACT OR GRANT NO. NASW-98004

12. SPONSORING AGENCY NAME AND ADDRESS Solar Physics Branch Code SS NASA Headquarters Washington, DC 20546	13. TYPE OF REPORT AND PERIOD COVERED Quarterly progress report: 12 February 1999 - 11 February 2000 14. SPONSORING AGENCY CODE NASA HQ/ CODE SS

15. SUPPLEMENTARY NOTES

16. ABSTRACT

The purpose of this investigation is to develop a new model for the acceleration of the fast solar wind by nonlinear, time-dependent multidimensional MHD simulations of waves in solar coronal holes. Preliminary computational studies indicate that solitary-like waves are generated in coronal holes nonlinearly by torsional Alfv\'{e}n waves. These waves in addition to thermal conduction may contribute considerably to the accelerate the solar wind. Specific goals of this proposal are to investigate the generation of nonlinear solitary-like waves and their effect on solar wind acceleration by numerical 2.5D MHD simulation of coronal holes with a broad range of plasma and wave parameters; to study the effect of random disturbances at the base of a solar coronal hole on the fast solar wind acceleration with a more advanced 2.5D MHD model and to compare the results with the available observations; to extend the study to a full 3D MHD simulation of fast solar wind acceleration with a more realistic model of a coronal hole and solar boundary conditions. The ultimate goal of the three year study is to model the fast solar wind in a coronal hole, based on realistic boundary conditions in a coronal hole near the Sun, and the coronal hole structure (i.e., density, temperature, and magnetic field geometry) that will become available from the recently launched SOHO spacecraft.

17. KEY WORDS (SUGGESTED BY AUTHOR(S)) Solar Wind Corona, MHD, Coronal Holes	18. DISTRIBUTION STATEMENT Space Science, Solar Physics

19. SECURITY CLASSIF. None	20. SECURITY CLASSIF. None	21. NO OF PAGES	22. PRICE